Optoelectrical Molybdenum Disulfide (MoS_2)—Ferroelectric Memories

Alexey Lipatov,[†] Pankaj Sharma,[‡] Alexei Gruverman,[‡,§] and Alexander Sinitskii[*,†,§]

[†]Department of Chemistry, [‡]Department of Physics and Astronomy, and [§]Nebraska Center for Materials and Nanoscience, University of Nebraska, Lincoln, Nebraska 68588, United States

ABSTRACT In this study, we fabricated and tested electronic and memory properties of field-effect transistors (FETs) based on monolayer or few-layer molybdenum disulfide (MoS_2) on a lead zirconium titanate ($Pb(Zr,Ti)O_3$, PZT) substrate that was used as a gate dielectric. MoS_2—PZT FETs exhibit a large hysteresis of electronic transport with high ON/OFF ratios. We demonstrate that the interplay of polarization and interfacial phenomena strongly affects the electronic behavior and memory characteristics of MoS_2—PZT FETs. We further demonstrate that MoS_2—PZT memories have a number of advantages and unique features compared to their graphene-based counterparts as well as commercial ferroelectric random-access memories (FeRAMs), such as nondestructive data readout, low operation voltage, wide memory window and the possibility to write and erase them both electrically and optically. This dual optoelectrical operation of these memories can simplify the device architecture and offer additional practical functionalities, such as an instant optical erase of large data arrays that is unavailable for many conventional memories.

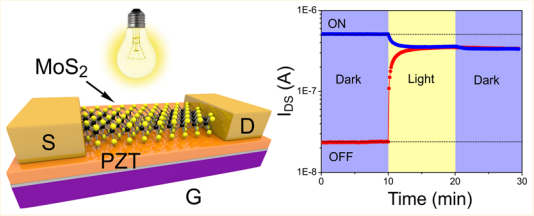

KEYWORDS: molybdenum disulfide · lead zirconium titanate · ferroelectric memory · field-effect transistor · hysteresis

Over the past few years, there has been considerable interest in electronic devices, in which graphene, a two-dimensional (2D) carbon allotrope,[1] was coupled with different ferroelectric materials, such as poly(vinylidene fluoride-trifluoroethylene) [P(VDF-TrFE)],[2−8] lead zirconium titanate ($Pb(Zr,Ti)O_3$, PZT)[9−15] and other complex oxides with perovskite structure.[16−18] Most of these studies have focused on the memory and logic applications of ferroelectric field-effect transistors (FeFETs) with graphene conducting channels and ferroelectric materials as gate dielectrics.[19] In these devices, the high ("ON") and low ("OFF") conductivity states of graphene were achieved by controlling the polarization of a ferroelectric material through the application of a necessary gate voltage. It is important to point out early that, for nonvolatile memory applications, a device should be bistable, that is, ON and OFF states should be achieved at the same gate voltage, V_G (which could be set to zero).[20] As a result, such memory ON/OFF ratio is smaller than the ratio of maximum and minimum drain-source (I_{DS}) currents observed in an $I_{DS}-V_G$ dependence, which would be considered as an ON/OFF ratio in graphene FET studies.[21] In this paper on memory devices, we exclusively use ON/OFF ratios for ON and OFF states achieved at the same V_G.

While the ferroelectric properties of a dielectric material are important to achieve stable nonvolatile ON and OFF states, the actual ON/OFF ratios in these devices depend on the intrinsic electronic properties of a channel material, graphene. Since graphene is a zero-band gap semiconductor, it remains highly conductive at any doping level.[1] As a result, for the FETs with monolayer graphene channels high ON/OFF ratios are difficult to achieve, which remains true when ferroelectric gating is used—in graphene-ferroelectric devices the previously reported ON/OFF ratios of drain currents measured at the same gate voltage range from 1.3 to 4,[10−12,14,15] while much higher values are necessary for most practical applications.

The drain current ON/OFF ratio of the FET devices can be significantly improved if graphene is replaced with a different 2D material that has a substantial electronic band gap. Molybdenum sulfide (MoS_2), a layered material that has recently received a great deal of attention,[22−28] could be a viable option. Bulk MoS_2 is a semiconductor with an indirect band gap of 1.2 eV, while monolayer MoS_2 is a semiconductor with a

* Address correspondence to sinitskii@unl.edu.

Received for review April 7, 2015 and accepted July 21, 2015.

Published online July 29, 2015
10.1021/acsnano.5b02078

direct band gap of 1.8 eV.[22] As a result, the drain currents in FETs with either monolayer or few-layer MoS_2 channels could vary by up to 8 orders of magnitude at room temperature.[26] Another practically important feature of MoS_2–PZT FETs is based on the unique optoelectronic properties of molybdenum disulfide.[29] We demonstrate that, in the MoS_2–PZT FeFETs, the data can be written and erased both electrically and optically, which can dramatically simplify the device architecture and enable instant optical erase of large data arrays that is unavailable for many conventional memories.

While MoS_2–PZT FeFET memories are superior to their graphene-based counterparts, they may also be considered as an alternative to the established ferroelectric-based memory technology, ferroelectric random access memories (FeRAMs), which incorporate ferroelectric capacitors.[30,31] In FeRAM devices, the stored data are read by applying a voltage pulse with amplitude above the coercive bias to determine the direction of polarization. As a result, a data bit has to be reprogrammed after each read, which leads to large read time and large power consumption. In contrast, in a FeFET memory, the read operation, which is performed by measuring the polarization-dependent in-plane transport, is nondestructive. Also, because of the strong covalent bonds between molybdenum and sulfur the MoS_2/PZT interfaces are expected to have a high chemically stability. This property may potentially address a major problem of integration of the FeFET devices into CMOS technology, which is associated with the difficulty to achieve ferroelectric/silicon interfaces of high structural quality. Despite some recent advances,[32−34] controlling the interfacial oxide layer formation and minimizing the interdiffusion of the constituent elements across the semiconductor-ferroelectric interface are still very serious challenges. In addition, the presence of an interfacial dielectric layer affects functionality of Si-based FeFETs due to the increased polarization instability.[35] Implementation of MoS_2, a stable 2D single-crystalline material, in ferroelectric memories could result in highly stable interfaces and a better resistance to the degradation effects.[36]

In addition to the technological potential of MoS_2–PZT FeFETs, this study also has an important fundamental component. Previously studied graphene-PZT devices exhibited an unusual electronic behavior that was not completely understood. In particular, several groups have reported that graphene–PZT FeFETs exhibit an unusual clockwise hysteresis of electronic transport, in contradiction with counterclockwise polarization dependence of PZT.[10,12,14,15] We demonstrate that interfacial charges have a strong effect on the hysteresis of electronic transport in MoS_2–PZT FeFETs, and the charge dissipation changes the hysteresis shape. This study shows that understanding the nature of this effect is important for devices comprising 2D materials on ferroelectric substrates in general. We investigated how the interplay of polarization and interfacial phenomena affects the electronic behavior and memory characteristics of MoS_2–PZT FETs, explain the origin of unusual clockwise hysteresis and experimentally demonstrate a reversed polarization-dependent hysteresis of electronic transport.

RESULTS AND DISCUSSION

MoS_2 flakes on Si/SiO_2 substrates were prepared by micromechanical exfoliation from a MoS_2 single crystal.[23] The flakes were found by optical microscopy (Figure 1a) and the number of MoS_2 layers in each flake was determined by Raman spectroscopy.[37] Figure 1b shows Raman spectrum of a MoS_2 flake presented in Figure 1a. The spectrum reveals the presence of two major lines at 382.1 cm^{-1} (E^1_{2g}) and 405.2 cm^{-1} (A_{1g}). The spectral positions of these lines indicate that this particular MoS_2 flake consists of three layers.[37] This flake was used for the device fabrication (Figure 1c) and electrical measurements. While this paper focuses on the electronic properties of a MoS_2–PZT FeFET based on the trilayer MoS_2 flake shown in Figure 1, we also fabricated and tested similar devices based on monolayer and bilayer MoS_2 flakes; see Supporting Information Figure 1. Overall, we did not observe a substantial difference between the electronic/memory properties of MoS_2–PZT FeFETs based on MoS_2 flakes comprising one, two, or three layers.

Details for the fabrication of bottom-gated MoS_2–PZT FeFETs are given in the Materials and Methods section. MoS_2 flakes with different thicknesses were transferred to a PZT substrate as shown in Figure 1c. First, Si/SiO_2 substrate with MoS_2 flake was covered with a film of poly(methyl methacrylate) (PMMA), and SiO_2 layer was dissolved using 5% aqueous solution of hydrofluoric acid (HF). Floating PMMA/MoS_2 film was then washed in DI water several times, transferred to a PZT substrate and dried in air, and PMMA was dissolved in acetone. Finally, Ti/Au electrodes were fabricated using electron-beam lithography. Figure 1d shows the scheme of a MoS_2-based FeFET on a ferroelectric substrate where Ti/Au source (S) and drain (D) electrodes are bridged by a MoS_2 flake. Figure 1e,f shows atomic force microscopy (AFM) images of a device based on the trilayer MoS_2 flake presented in Figure 1a; this device was used for most measurements reported in this paper. Polycrystalline 100 nm thick (001)-oriented tetragonal $PbZr_{0.4}Ti_{0.6}O_3$ films used in this work were grown by metal–organic chemical vapor deposition on a silicon wafer covered with a conductive TiO_2/Ir layer used as a back gate (G) electrode (Figure 1d); the Curie temperature of these PZT films is about 360 °C. Polycrystalline nature of the PZT substrate can be seen in Supporting Information Figure 2b and in Figure 1f, where numerous grains of less than 100 nm in size can

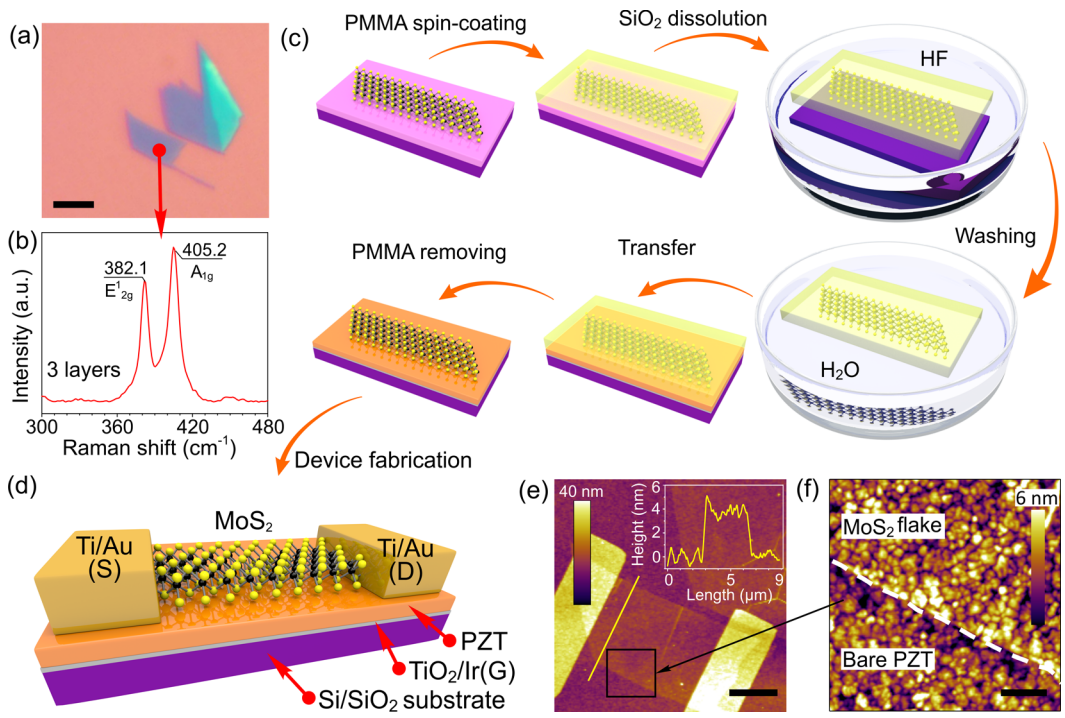

Figure 1. Fabrication of MoS_2-based FeFETs. (a) Optical image of a three-layer MoS_2 flake on Si/SiO_2 substrate. Scale bar is 5 μm. (b) Raman spectrum of the MoS_2 flake shown in (a). (c) Scheme of the fabrication of MoS_2-based FeFETs; see text for details. (d) Scheme of a MoS_2-based FeFET. (e,f) AFM images of the device shown in (a). Scale bars are 2 μm and 500 nm, respectively. Inset in (e) shows the height profile along the yellow line.

be observed. The rms roughness measured for the bottom part of the PZT surface in Figure 1f that was not covered by the MoS_2 flake is 5.4 $\pm$ 1.4 nm. The presence of a trilayer MoS_2 flake makes the surface noticeably smoother, as the rms roughness measured for the top part of the PZT surface in Figure 1f that was covered by the MoS_2 flake is 3.6 $\pm$ 1.3 nm. However, because of the substantial roughness of the substrate the PZT grains can be seen in an AFM image even through a trilayer MoS_2 flake. Results of ferroelectric testing of the PZT films by Sawyer–Tower method and piezoresponse force microscopy (PFM) are presented in Supporting Information Figure 2 and Note 1.

Electrical measurements of MoS_2-based FETs were performed in vacuum ($p \sim 1 \times 10^{-6}$ Torr) after 2 days of evacuation to minimize the effect of surface adsorbates.[38] Figure 2a shows the $I_{DS}-V_G$ dependence measured at drain-source voltage (V_{DS}) of 0.1 V for the MoS_2–PZT FeFET shown in Figure 1e; the same dependence in logarithmic I_{DS} coordinates is shown in Supporting Information Figure 3a. There is a significant difference between $I_{DS}-V_G$ curves measured when V_G was swept from −6 to +6 V (blue line) and from +6 to −6 V (red line), which results in a very large hysteresis of the electronic transport. While similar graphene–PZT devices typically have ON/OFF ratios ranging from 1.3 to 4,[10−12,14,15] in this MoS_2–PZT FeFET the ON/OFF ratio at $V_G = -1.1$ V is 205 (see Supporting Information Figure 3a) which shows the potential of MoS_2-based FeFETs for memory applications.

The shape of the conductivity hysteresis depends on a number of measurement parameters. Supporting Information Figure 3c shows that it strongly depends on the V_G sweep rate: the faster the measurement, the larger the hysteresis. The electronic behavior of MoS_2-based FeFETs is further affected by visible light illumination, as shown in Supporting Information Figure 3d. We discuss the usefulness of this effect below, but it is important to point out that all electrical measurements shown in this paper were performed in darkness unless indicated otherwise.

Figure 2a shows pronounced I_{DS} peaks in the $I_{DS}-V_G$ curve at $V_G = -2.9$ and +2.3 V, which correspond to the voltages at which polarization reversal of the PZT substrate occurs (these voltages are close to those observed by means of PFM switching spectroscopy; see Supporting Information Figure 2c). Similar features are also observed in the drain-gate current (I_{DG})–V_G dependence (Figure 2b) as the structural transformations in PZT during the polarization reversals result in increased leakage current through the substrate. Similar maxima at comparable gate voltages were observed in graphene-PZT devices and also attributed to the polarization reversals in a ferroelectric film.[14]

Analysis of Figure 2a shows that while polarization of PZT is manifested in the $I_{DS}-V_G$ curves, it is not the only factor affecting the electronic behavior of MoS_2–PZT FeFETs. One unusual feature that has been previously reported for graphene-PZT devices is that the observed hysteresis has a clockwise direction, which does

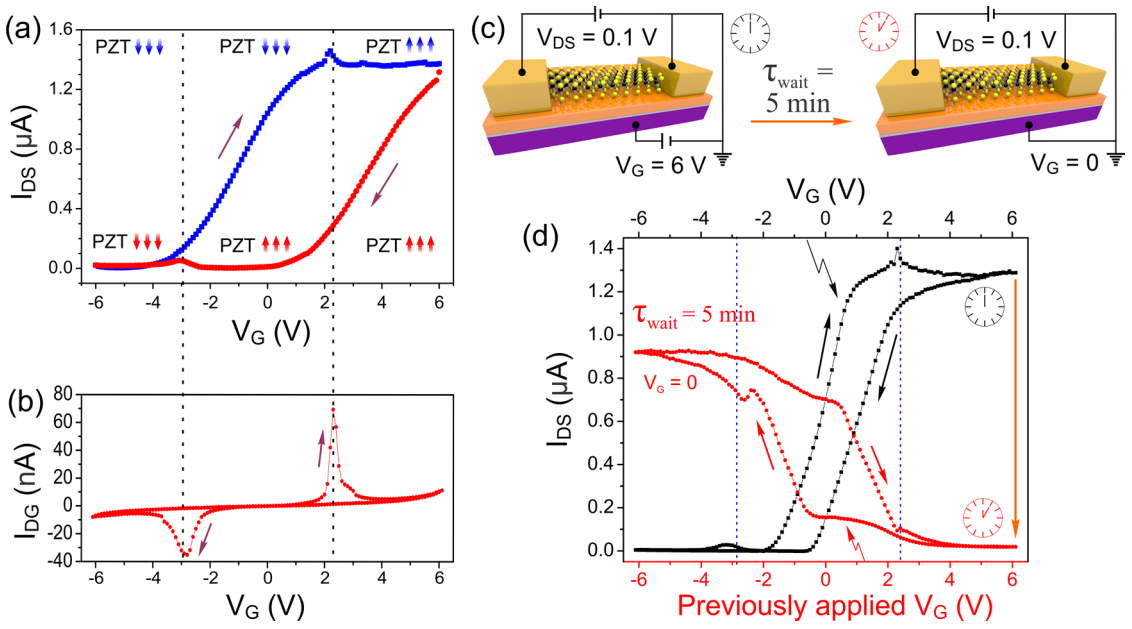

Figure 2. Electronic properties of a MoS_2-PZT FeFET. In all measurements shown V_{DS} = 0.1 V. (a) $I_{DS}-V_G$ characteristics for the device shown in Figure 1e. The arrows in the insets show the polarization directions of PZT at different V_G, which were determined from PFM measurements; see Supporting Information Figure 2 and Note 1. (b) V_G dependence of the drain-gate (leakage) current ($I_{DG}-V_G$ measurements) for the same device. (c) Scheme of the electrical measurements revealing the polarization-dependent hysteresis of electronic transport in MoS_2–PZT FeFETs; see text for details. (d) $I_{DS}-V_G$ characteristics for the same device measured using the method shown in (c). Black data points show I_{DS} values while V_G was applied; see the top horizontal axis. Red data points show I_{DS} values measured at grounded gate voltage (V_G = 0) 5 min after the corresponding gate voltages were applied; see the bottom horizontal axis. Arrows indicate the directions of hystereses.

not agree with the counterclockwise polarization hysteresis of PZT (see Supporting Information Figure 2a). The shape of the observed $I_{DS}-V_G$ hysteresis also raises a number of questions. As the PZT polarization reversals occur at $V_G = -2.9$ and +2.3 V, we can distinguish three different V_G regions in the transfer characteristics of a MoS_2–PZT FeFET (Figure 2a). At $V_G > +2.3$ V, the polarization of PZT is always up regardless of the V_G sweep direction; at $V_G < -2.9$ V, the polarization of PZT is always down; and for -2.9 V $< V_G < +2.3$ V, the polarization could be directed either way depending on the direction of V_G sweep; the corresponding polarization directions are shown in the insets in Figure 2a. If PZT polarization was the only factor affecting the electronic behavior of a MoS_2–PZT FeFET, at gate voltages > +2.3 V the drain-source current values would be the same for both V_G sweep directions. On the contrary, while in the forward sweep I_{DS} saturates at ~1.3 μA once the gate voltage exceeds +2.3 V, it rapidly decays in the reverse V_G sweep. Furthermore, as we show in Supporting Information Figure 3c, the hysteresis shape (in particular, the I_{DS} slope for the V_G sweep from +5 to −3 V) strongly depends on the gate voltage sweep rate, suggesting the kinetic nature of the effect. Similarly, the I_{DS} values also vary for different V_G sweep directions at $V_G < -2.9$ V (see the $I_{DS}-V_G$ characteristics for the same device shown in semilogarithmic coordinates in Supporting Information Figure 3a), and therefore are not affected only by the polarization of PZT either.

The electrical behavior of MoS_2 devices on PZT substrates can be complicated by charge injection.[39] As a result, when V_G is applied, a PZT film accumulates interfacial charges that may remain on a surface for some time even after gate voltage is removed. The fact that the slope of the $I_{DS}-V_G$ curve depends on the speed of measurement indicates that the observed hysteresis may be affected by the interfacial charges. Previous studies also suggested that the unusual clockwise hysteresis of the conductivity of graphene-PZT devices may be caused by the trapped charges at the interface between graphene and PZT.[10,12,40] Therefore, it is very likely that $I_{DS}-V_G$ dependencies that were previously measured for graphene-PZT devices and also shown for MoS_2–PZT FeFETs in this work (Figure 2a) manifest an interplay of at least two different effects: a polarization of the ferroelectric substrate and charge traps at the interface between a substrate and a 2D material.

In order to separate the effects of PZT polarization and interfacial charges on MoS_2 conductivity, we designed the following experiment (Figure 2c). First, we apply V_G = +6 V, at which the PZT substrate has a stable upward polarization for 1 ms, and measure I_{DS} while V_G is applied. The resulting drain-source current of 1.3 μA represents the effects of both PZT polarization and interfacial charges on the conductivity of MoS_2. Then, we remove the gate voltage, wait for τ_{wait} = 5 min, and then measure I_{DS} again, this time without the gate voltage applied (*i.e.*, at V_G = 0). As a result, the drain-source current decreases by 2 orders of

magnitude compared to the measurement when $V_G = +6$ V was applied; the change in I_{DS} is shown by the arrow in Figure 2d. In the same manner, we swept V_G from +6 to −6 V and back, and at each gate voltage we obtained two I_{DS} values, one while V_G was applied and another 5 min later at $V_G = 0$. These measurements resulted in two $I_{DS}-V_G$ dependencies that are shown in Figure 2d. The black hysteresis loop where I_{DS} values were measured while V_G was applied shows how the conductivity of MoS_2 is affected by both the PZT polarization and the interfacial charges. Since τ_{wait} = 5 min is a sufficient time for a substantial amount of interfacial charges to dissipate (this is discussed in Supporting Information Note 2), the red curve in Figure 2d, for which I_{DS} values were measured 5 min after V_G was applied, shows the MoS_2 conductivity that is primarily affected by the polarization of PZT while the effect of interfacial charges is minimized.

The black and red hysteresis loops in Figure 2d look dramatically different. First of all, once the effect of the charge traps is minimized, the hysteresis reverses (red curve in Figure 2d). An interesting outcome of this hysteresis reversal is that the conductivity of a MoS_2/PZT FeFET changes from n- to p-type. Although there are precedents of p-type MoS_2 transistors enabled by high work function contacts[41] and substitutional doping,[42] in our case the observed p-type transport is likely caused by the MoS_2−substrate interaction.[43] While the exact origin of the p-type conductivity of MoS_2/PZT FeFETs after the interfacial charge dissipation can be a subject of a separate study, for memory applications of these devices the reversed hysteresis is important for showing nonvolatile ON and OFF states. In this polarization-controlled MoS_2 conductivity hysteresis the PZT polarization reversals at $V_G = -2.9$ and +2.3 V clearly mark three different V_G regions, as expected. In red curve in Figure 2d, for any $V_G > +2.3$ V or < -2.9 (when the polarization of PZT is either up or down, respectively) the I_{DS} values for the forward and reverse V_G sweep directions are very similar, which is different from the previously discussed case when the charge trap effects were not eliminated (see Figure 2a and the black hysteresis in Figure 2d). As expected, in the polarization-controlled conductivity hysteresis substantially different I_{DS} values can be achieved only in the operation window of -2.9 V $< V_G < +2.3$ V, where the polarization of PZT could be either up or down depending on the V_G sweep direction. It is important to note that such a wide memory window (width of the $I_{DS}-V_G$ loop) of over 4 V is a necessary condition for strong retention of nonvolatile FeFET devices, as it ensures a stable polarization, and large drain current ON/OFF ratio. For comparison, the memory window of the FeFET based on $SrBi_2Ta_2O_9$ ferroelectric films is only 1.6 V at $V_G = 1.7$ V.[44]

Additional electrical measurements of MoS_2−PZT FeFETs can be found in Supporting Information Figure 4 with accompanying details provided in Supporting Information Note 2. In particular, conductivity hysteresis loops measured at different τ_{wait} confirm that a substantial amount of interfacial charges dissipate in less than 5 min. Supporting Information Figure 4 further shows the comparison of the MoS_2−PZT FeFETs based on monolayer, bilayer, and trilayer MoS_2 flakes; all these devices exhibit qualitatively similar electronic behavior.

The demonstration of the reversed conductivity hysteresis in MoS_2-based FeFETs is important not only for the fundamental understanding of the interplay of PZT polarization and charge traps, but also for practical memory applications. The current values extracted from the hysteresis loops, such as the one shown in Figure 2a, cannot be considered for the long-term data storage, as they are affected by the interfacial charges, and will change as these charges dissipate. In contrast, a conductivity hysteresis measured as described in Figure 2c shows a correct memory operation; see Figure 3a. In the following example, all operations (write, erase, read) were performed at $V_{DS} = 0.1$ V. The hysteresis in Figure 3a shows all memory states that could be realized in a MoS_2−PZT FeFET at $V_G = 0$ after $\tau_{wait} = 5$ min. A high conductivity (ON state) can be achieved at grounded gate if a negative gate voltage below −2.9 V is first applied; in this example, we selected $V_G = -6$ V as the "write" voltage (Figure 3a). Conversely, if a positive gate voltage over +2.3 V is applied, a low conductivity OFF state will be realized; in this example, we used $V_G = +6$ V as the "erase" voltage (Figure 3a).

In order to study the effect of interfacial charges on the retention characteristics of ON and OFF states, we first applied either "write" (−6 V) or "erase" (+6 V) gate voltage and then read I_{DS} at $V_G = 0$ every 6 s for 10^4 s; see Figure 3b. The ON/OFF ratio measured at $V_G = 0$ six seconds after ON and OFF states were recorded is 10^4. However, as we discuss above, the I_{DS} values are originally affected by both the polarization of PZT and the charge traps. As the interfacial charges dissipate over time, the ON and OFF current values change, as shown in Figure 3b. Mostly due to the increase in the OFF current, the ON/OFF ratio decreases down to ~22 after 10^4 s. This graph also shows that a substantial amount of interfacial charges dissipates in 5 min, although the complete change dissipation requires a much longer time. Note that $I_{DS}-V_G$ hysteresis dependencies measured at τ_{wait} = 5 min and 30 min are qualitatively similar, see Supporting Information Figure 4 and Note 2.

Figure 3c shows the results of the MoS_2−PZT memory endurance test using 500 "erase−read−write−read" cycles. Write and erase operations were performed by applying $V_G = -6$ or +6 V, respectively, for 1 ms, and the reading was performed by measuring I_{DS} values 16 s later at $V_G = 0$. Figure 3c shows that the memory operation was very stable, as neither ON nor OFF currents changed over 500 cycles. During the

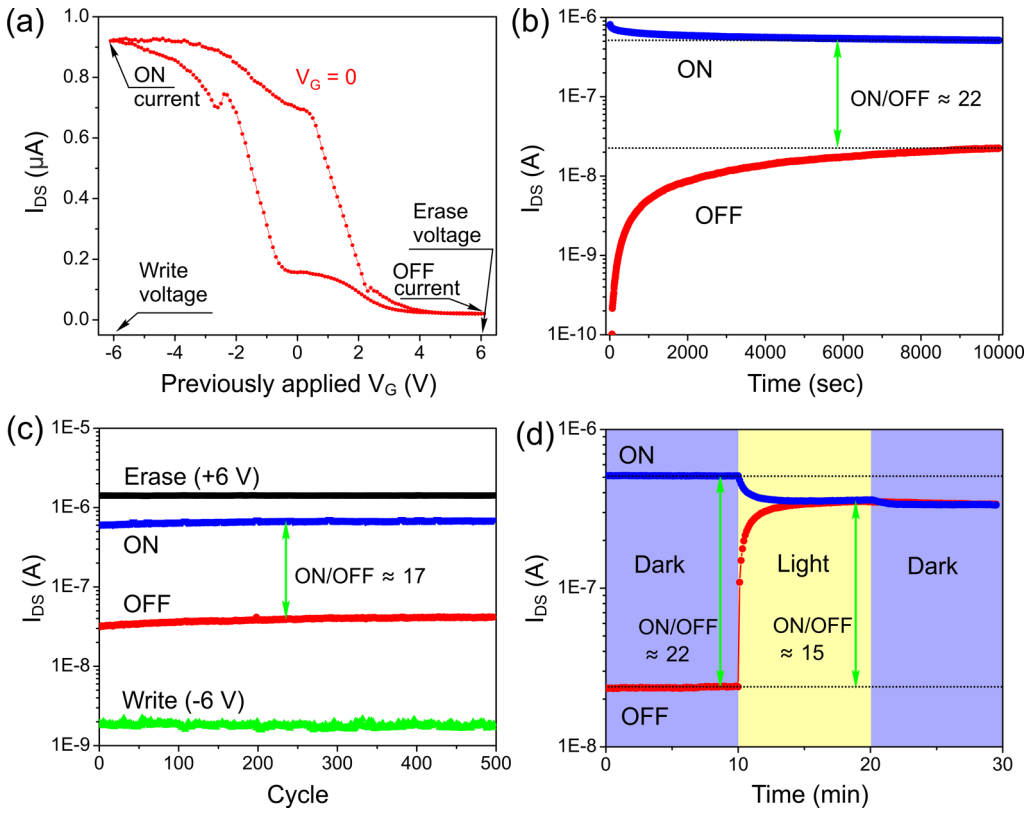

Figure 3. Memory properties of MoS_2-PZT FeFET. In all measurements shown, V_{DS} = 0.1 V. (a) Polarization-dependent hysteresis of electronic transport in a MoS_2−PZT FeFET that was measured using the method shown Figure 2c. Arrows show write and erase voltages and the corresponding ON and OFF currents. (b) Data retention characteristics of a MoS_2−PZT FeFET. After application of the write (V_G = −6 V) and erase (V_G = +6 V) voltages, the ON and OFF drain-source currents at V_G = 0 were measured as a function of time. (c) Cyclic endurance of the same device: pulses of −6 and 6 V for 1 ms were used for writing and erasing, respectively. After each write/erase operation, the I_{DS} current was read after τ_{wait} = 16 s at V_G = 0. (d) Effect of visible light illumination on the data retention characteristics of a MoS_2−PZT FeFET; see text for details.

memory endurance test, the ON/OFF ratio of the MoS_2−PZT device remained at 17, which is significantly higher than the drain current ON/OFF ratios in graphene FeFETs, especially if the readings are performed at the same gate voltage.[10−12,14,15] While this graph shows the cycle endurance of the MoS_2−PZT memory, the actual ON/OFF ratio may vary in different measurements, as it is a function of both the duration of the V_G pulse and τ_{wait}.

Because of the semiconductor nature of molybdenum disulfide,[26,29] MoS_2−PZT memories have a number of other unique properties compared to previously reported graphene FeFETs.[10−12,14,15] If MoS_2−PZT structures are illuminated with a visible light, the photogenerated charge carriers in molybdenum disulfide can produce an electric field that would affect polarization of PZT underneath the MoS_2 flake. This opens a possibility of eliminating the difference between ON and OFF states by the exposure of a device to light. Figure 3d demonstrates the implementation of this effect in a MoS_2−PZT memory device. As in the previous examples (Figure 3a−c), ON and OFF states were generated by applying either "write" (−6 V) or "erase" (+6 V) gate voltages, respectively, and I_{DS} values were read at V_G = 0 in darkness until the ON and OFF currents stabilized (Figure 3b). Figure 3d shows that the I_{DS} values were stable for at least 10 min until the device was illuminated with a light of a 150 W halogen bulb, which resulted in the degradation of both ON and OFF states. After 5 min of light exposure, the ON and OFF states were completely indistinguishable, and when the light was turned off, the original ON and OFF states were not restored (Figure 3d). This experiment shows that a MoS_2−PZT memory can be completely erased simply by exposure to light.

In order to get a deeper insight into the optically induced erasure of the ON and OFF states, we tested the polarization of PZT covered with a trilayer MoS_2 flake using PFM with and without light illumination (Figure 4a−d). PFM images of the MoS_2−PZT device acquired in the dark after poling by a positive pulse of +5 V through a PFM tip are shown in Figure 4a,b. The PZT film under the MoS_2 flake is fully polarized downward and exhibits a strong PFM amplitude signal and bright PFM phase contrast. Note that the uncovered area of PZT retains downward polarization illustrating the fact that the polarization reversal occurred only underneath the MoS_2 flake, which serves as a top electrode (see Supporting Information Figure 5 and Note 3); the polarization reversal behavior of

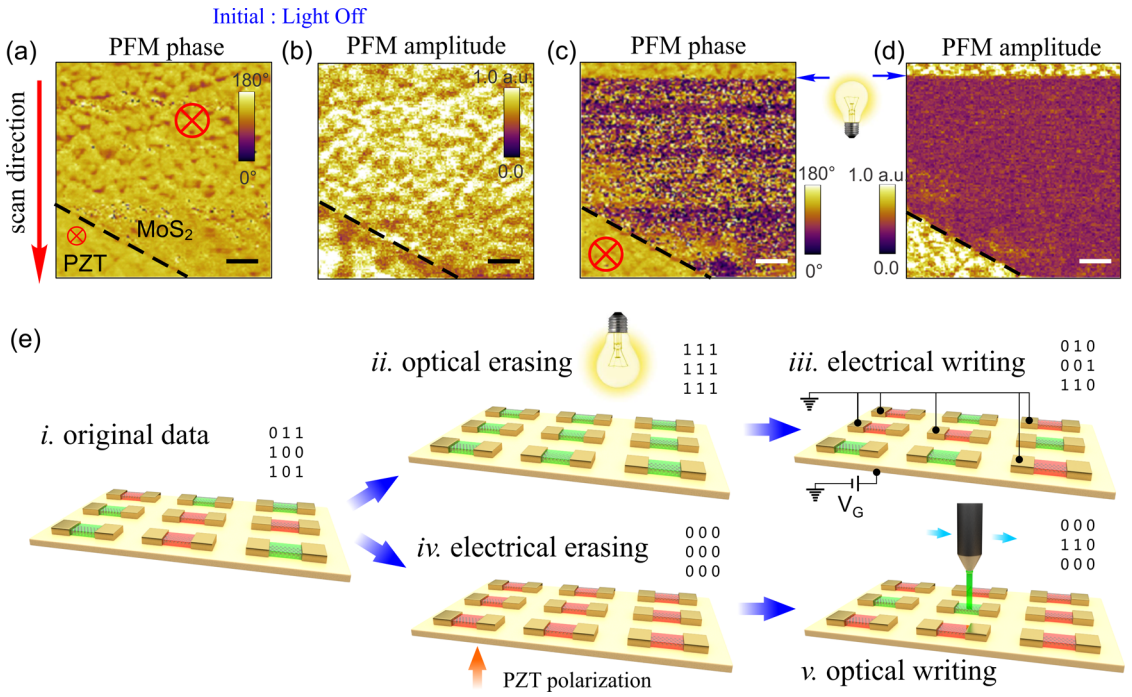

Figure 4. Optical switching of MoS_2-PZT memories. (a, b) PFM phase (a) and amplitude (b) images obtained after application of +5 V pulse to the MoS_2 flake. The images were recorded in the dark. (c, d) PFM phase (c) and amplitude (d) images of the same area as in (a, b) measured first in the dark (top parts of the images) and then with a visible light illumination (bottom parts of the images). The moment when the light was turned on is indicated by the blue arrows. Dashed black lines in images (a)–(d) show the edge of the MoS_2 flake. Scale bars are 200 nm. (e) "Optical erase–electrical write" and "electrical erase–optical write" operation of MoS_2–PZT memories.

graphene-ferroelectric tunneling junctions is discussed in detail in our recent study.[45] Figure 4c,d shows PFM images of the same area of the MoS_2–PZT device where the scanning was started from the top of the image in the darkness and then the light was turned on at the moment indicated by the blue arrows. An abrupt decrease in the PFM amplitude signal (appearing as a change in contrast from bright to dark) might be an indication of a significantly reduced net polarization due to the formation of a number of antiparallel domains. This optically induced domain rearrangement could be a result of the less efficient screening of the downward polarization in PZT by the photogenerated electrons. This results in a transition from a single-domain to polydomain state as a way to minimize the depolarizing field energy.[46,47] This polydomain structure of the PZT substrate below the MoS_2 channel may cause an intermediate resistance of a device that is different from both ON and OFF states. Another possible mechanism for the reduced PFM amplitude could be the optically induced changes in the electrical properties of the MoS_2 flake and/or MoS_2/PZT interface. The exact mechanism is still to be clarified and is a subject of the ongoing investigation. Note that the light illumination only affects the polarization of PZT substrate below the MoS_2 flake, while outside of the flake the downward polarization persists (Figure 4c,d), which further shows that the described effect is caused by the photogenerated charge carriers in MoS_2.

The PFM data show that illumination of a MoS_2–PZT FeFET with visible light affects both OFF and ON states of a device. However, the conductivity of the optically erased state of the device is much closer to the original ON state than to the original OFF state (Figure 3d). Therefore, for practical purposes, the optically erased state can still be considered as an "ON" state. For the device shown in Figure 3d, this notation decreases the ON/OFF ratio from 22 to 15, which is still acceptable for many practical applications. The ability of setting a MoS_2–PZT FeFET to the ON state by illumination with visible light opens a number of previously inaccessible opportunities with data recording and erasing.

Figure 4e shows two different schemes of optoelectrical operation of MoS_2–PZT memories. The schematic (i) shows an array of MoS_2–PZT FeFETs where each device is prerecorded in either ON ("1") or OFF ("0") state. The entire array can be simultaneously erased optically by setting all devices to ON state via light illumination (ii). Such instant erase is currently elusive for many conventional memory technologies, and particularly attractive for high-capacity data storage systems (in comparison, it takes several hours to erase a modern 1 TB hard disk drive by individually rewriting every memory segment). Once the array of MoS_2–PZT FeFETs is optically erased (ii), the data can be written electrically by individually accessing the devices that need to be in the OFF state and polarizing the PZT substrate under these devices upward (iii).

In addition to the "optical erase−electrical write" operation of MoS_2−PZT memories, it is also possible to realize the "electrical erase−optical write" mode (Figure 4e). Starting with the same array of prerecorded MoS_2−PZT FeFETs (i), it is possible to erase it electrically (iv) by polarizing the entire PZT substrate upward using the global back gate (note that the PZT switching will occur only under the biased MoS_2 flakes, meaning that every device will need to be electrically accessed; this emphasizes the advantage of the optical erasing of MoS_2−PZT FeFETs (ii) where all illuminated devices are erased simultaneously). Then, the data can be written optically by individually illuminating the devices that need to be in the ON state using, for example, a focused laser beam (v). The demonstrated optical switching complements the conventional "electrical erase−electrical write" operation mode that can also be realized in these memories; see Figure 3.

CONCLUSIONS

In summary, we have fabricated MoS_2−PZT FeFET devices and demonstrated that they have a large hysteresis of electronic transport and promising memory properties. MoS_2−PZT devices share many similarities with graphene-PZT devices but have substantially higher ON/OFF ratios due to the semiconductor nature of MoS_2. We demonstrate that interfacial phenomena play an important role in the electronic behavior and memory characteristics of MoS_2−PZT FETs, and show a reversed polarization-dependent hysteresis of electronic transport. We further demonstrate that MoS_2−PZT memories have a number of advantages over commercial FeRAMs, such as nondestructive data readout, low operation voltage, wide memory window, and the possibility to write and erase them both electrically and optically. The unique dual optoelectrical switching of these memories that we demonstrate in this study opens new possibilities in the device architecture and operation. Finally, while previous works have focused on the devices comprising graphene and ferroelectric perovskites,[9−18] we demonstrate a great promise of layered heterostructures combining ferroelectric perovskites with other emerging 2D materials[48−51] for fundamental materials studies and device applications.

MATERIALS AND METHODS

Materials. MoS_2 single crystal (SPI supplies) and p-type silicon wafers covered with 300 ± 15 nm thick SiO_2 (Silicon Quest International) were used to prepare MoS_2 flakes. PMMA950 A4 (4% poly(methyl methacrylate) in anisole, MicroChem Corp.), methyl isobutyl ketone/isopropanol (1:3) (MIBK/IPA, MicroChem Corp.), isopropanol (IPA, Sigma-Aldrich, 99.5+%), and acetone (Fisher Scientific, 99.7%) were used as received for electron beam lithography to pattern the electrodes on MoS_2 flakes. Hydrofluoric acid (48 wt % in H_2O, ≥99.99% trace metals basis) for the transfer of MoS_2 flakes was purchased from Sigma-Aldrich. Titanium (Ti, 99.995%) and gold (Au, 99.999%) targets were purchased from International Advanced Materials and used for electron beam evaporation.

Device Fabrication. *MoS_2 Exfoliation.* MoS_2 flakes were exfoliated on the surface of a Si/SiO_2 substrate using an adhesive tape.[23] Ultrathin MoS_2 flakes were then identified by optical microscopy.

Transfer of MoS_2 Flakes to PZT Substrates. Si/SiO_2 substrate with MoS_2 flakes was covered with PMMA solution by spin-coating and dried in air. Then the substrate was placed on the surface of 5% HF aqueous solution for 1 min to etch away SiO_2 layer. The transparent MoS_2/PMMA film was then transferred to the surface of deionized (DI) water and floated there for 5 min. The washing of MoS_2/PMMA film with DI water was repeated three to four times and then the film was transferred to a PZT substrate. After drying in air at room temperature the sample was washed by hot (50 °C) acetone to remove PMMA layer, rinsed with isopropanol and water and dried with nitrogen gas.

Nanofabrication. PMMA was spin-coated on PZT substrate with MoS_2 flakes at 5000 rpm for 45 s. Then the substrate was placed on a hot plate at 180 °C for 120 s. Zeiss Supra 40 field-emission scanning electron microscope and a Raith pattern generator were used for electron beam lithography to pattern electrodes on a MoS_2 flake. After exposure, the substrate was developed in the MIBK/IPA mixture for 60 s, successively rinsed with 2-propanol and DI water, and then dried with nitrogen gas. AJA electron beam evaporation system at the base pressure of ~8×10^{-9} Torr was used to evaporate 2 nm of Ti at 0.1 Å/s rate, which was monitored by a quartz crystal microbalance. This was immediately followed by evaporation of 15 nm of Au at 0.2 Å/s rate. PMMA and excessive metals were removed by lift-off in hot acetone for 10 min. Finally, the substrate was rinsed with isopropanol and water, and dried with nitrogen gas.

Characterization of MoS_2 Flakes. *Raman Spectroscopy.* Raman spectra were recorded using a Thermo Scientific DXR Raman Microscope with a 532 nm excitation laser at a power level of 10.0 mW.

Scanning Electron Microscopy (SEM). SEM was performed using a Zeiss Supra 40 field-emission scanning electron microscope at the accelerating voltage of 5 kV.

Atomic Force Microscopy (AFM) and Piezoresponse Force Microscopy (PFM). Polarization imaging and local switching spectroscopy has been performed using a resonant-enhanced piezoresponse force microscopy (MFP-3D, Asylum Research). Conductive silicon cantilevers (PPP-EFM, Nanosensors) have been used in this study. PFM hysteresis loops were obtained at fixed locations on the junction surface as a function of switching pulses (12 ms) superimposed on ac modulation bias with amplitude of 0.6Vp-p at about 320 kHz. Tip contact forces have been calibrated by measuring force−distance curves and have been kept at a level of 20 nN.

Device Characterization. Electrical measurements were performed using a Lake Shore TTPX cryogenic probe station at the base pressure of 2×10^{-6} Torr. The device electrodes were connected to an Agilent 4155C semiconductor parameter analyzer that was linked to a computer through 82357B USB/GPIB interface and controlled using a National Instruments LabView code.

Conflict of Interest: The authors declare the following competing financial interest(s): A full patent application has been filed.

Supporting Information Available: Figures showing (1) SEM and optical images of the FeFETs fabricated using monolayer and bilayer MoS_2 flakes, their Raman spectra and transfer characteristics; (2) switching of ferroelectric polarization in a PZT film; (3) electronic properties of a trilayer MoS_2−PZT FeFET measured using various experimental conditions; (4) transfer characteristics of FeFETs based on mono-, bi-, and trilayer MoS_2 flakes measured using various τ_{wait}; (5) switching of ferroelectric polarization in a PZT film under a MoS_2 flake. Notes discussing (1) polarization switching in PZT films; (2) relaxation of the I_{DS} in

MoS_2—PZT FeFETs; (3) switching of the ferroelectric polarization in PZT under a MoS_2 flake. The Supporting Information is available free of charge on the ACS Publications website at DOI: 10.1021/acsnano.5b02078.

Acknowledgment. This work was supported by the National Science Foundation (NSF) through ECCS-1509874 with a partial support from the Nebraska Materials Research Science and Engineering Center (MRSEC) (Grant No. DMR-1420645). A.G. also acknowledges the support of Semiconductor Research Corporation Nanoelectronics Research Initiative (NRI) through the Center for NanoFerroic Devices (CNFD). This research was performed in part in Central Facilities of the Nebraska Center for Materials and Nanoscience (NCMN), which is supported by the Nebraska Research Initiative.

REFERENCES AND NOTES

1. Geim, A. K.; Novoselov, K. S. The Rise of Graphene. *Nat. Mater.* **2007**, *6*, 183–191.
2. Zheng, Y.; Ni, G.-X.; Toh, C.-T.; Zeng, M.-G.; Chen, S.-T.; Yao, K.; Özyilmaz, B. Gate-Controlled Nonvolatile Graphene-Ferroelectric Memory. *Appl. Phys. Lett.* **2009**, *94*, 163505.
3. Zheng, Y.; Ni, G.-X.; Toh, C.-T.; Tan, C.-Y.; Yao, K.; Özyilmaz, B. Graphene Field-Effect Transistors with Ferroelectric Gating. *Phys. Rev. Lett.* **2010**, *105*, 166602.
4. Doh, Y.-J.; Yi, G.-C. Nonvolatile Memory Devices Based on Few-Layer Graphene Films. *Nanotechnology* **2010**, *21*, 105204.
5. Ni, G.-X.; Zheng, Y.; Bae, S.; Tan, C. Y.; Kahya, O.; Wu, J.; Hong, B. H.; Yao, K.; Özyilmaz, B. Graphene—Ferroelectric Hybrid Structure for Flexible Transparent Electrodes. *ACS Nano* **2012**, *6*, 3935–3942.
6. Raghavan, S.; Stolichnov, I.; Setter, N.; Heron, J.-S.; Tosun, M.; Kis, A. Long-Term Retention in Organic Ferroelectric-Graphene Memories. *Appl. Phys. Lett.* **2012**, *100*, 023507.
7. Hwang, H. J.; Yang, J. H.; Lee, Y. G.; Cho, C.; Kang, C. G.; Kang, S. C.; Park, W.; Lee, B. H. Ferroelectric Polymer-Gated Graphene Memory with High Speed Conductivity Modulation. *Nanotechnology* **2013**, *24*, 175202.
8. Jandhyala, S.; Mordi, G.; Mao, D.; Ha, M.-W.; Quevedo-Lopez, M. A.; Gnade, B. E.; Kim, J. Graphene-Ferroelectric Hybrid Devices for Multi-Valued Memory System. *Appl. Phys. Lett.* **2013**, *103*, 022903.
9. Hong, X.; Posadas, A.; Zou, K.; Ahn, C. H.; Zhu, J. High-Mobility Few-Layer Graphene Field Effect Transistors Fabricated on Epitaxial Ferroelectric Gate Oxides. *Phys. Rev. Lett.* **2009**, *102*, 136808.
10. Hong, X.; Hoffman, J.; Posadas, A.; Zou, K.; Ahn, C. H.; Zhu, J. Unusual Resistance Hysteresis in n-Layer Graphene Field Effect Transistors Fabricated on Ferroelectric $Pb(Zr_{0.2}Ti_{0.8})O_3$. *Appl. Phys. Lett.* **2010**, *97*, 033114.
11. Zheng, Y.; Ni, G. X.; Bae, S.; Cong, C. X.; Kahya, O.; Toh, C. T.; Kim, H. R.; Im, D.; Yu, T.; Ahn, J. H.; Hong, B. H.; Özyilmaz, B. Wafer-Scale Graphene/Ferroelectric Hybrid Devices for Low-Voltage Electronics. *EPL* **2011**, *93*, 17002.
12. Song, E. B.; Lian, B.; Kim, S. M.; Lee, S.; Chung, T. K.; Wang, M. S.; Zeng, C. F.; Xu, G. Y.; Wong, K.; Zhou, Y.; Rasool, H. I.; Seo, D. H.; Chung, H. J.; Heo, J.; Seo, S.; Wang, K. L. Robust bi-stable memory operation in single-layer graphene ferroelectric memory. *Appl. Phys. Lett.* **2011**, *99*, 042109.
13. Hong, X.; Zou, K.; DaSilva, A. M.; Ahn, C. H.; Zhu, J. Integrating Functional Oxides with Graphene. *Solid State Commun.* **2012**, *152*, 1365–1374.
14. Baeumer, C.; Rogers, S. P.; Xu, R. J.; Martin, L. W.; Shim, M. Tunable Carrier Type and Density in Graphene/$PbZr_{0.2}Ti_{0.8}O_3$ Hybrid Structures through Ferroelectric Switching. *Nano Lett.* **2013**, *13*, 1693–1698.
15. Lee, W.; Kahya, O.; Toh, C. T.; Özyilmaz, B.; Ahn, J.-H. Flexible graphene—PZT ferroelectric nonvolatile memory. *Nanotechnology* **2013**, *24*, 475202.
16. Jung, I.; Son, J. Y. A Nonvolatile Memory Device Made of a Graphene Nanoribbon and a Multiferroic $BiFeO_3$ Gate Dielectric Layer. *Carbon* **2012**, *50*, 3854–3858.
17. Jie, W. J.; Hui, Y. Y.; Chan, N. Y.; Zhang, Y.; Lau, S. P.; Hao, J. H. Ferroelectric Polarization Effects on the Transport Properties of Graphene/PMN-PT Field Effect Transistors. *J. Phys. Chem. C* **2013**, *117*, 13747–13752.
18. Rajapitamahuni, A.; Hoffman, J.; Ahn, C. H.; Hong, X. Examining Graphene Field Effect Sensors for Ferroelectric Thin Film Studies. *Nano Lett.* **2013**, *13*, 4374–4379.
19. Jie, W.; Hao, J. Graphene-Based Hybrid Structures Combined with Functional Materials of Ferroelectrics and Semiconductors. *Nanoscale* **2014**, *6*, 6346–6362.
20. Crippa, L.; Micheloni, R.; Motta, I.; Sangalli, M., Nonvolatile Memories: NOR vs. NAND Architectures. In *Memories in Wireless Systems*; Micheloni, R.; Compardo, G., Olivo, P., Eds.; Springer-Verlag: Berlin, Heidelberg, 2008; pp 29—53.
21. Xia, F.; Farmer, D. B.; Lin, Y.-m.; Avouris, P. Graphene Field-Effect Transistors with High On/Off Current Ratio and Large Transport Band Gap at Room Temperature. *Nano Lett.* **2010**, *10*, 715–718.
22. Kato, T.; Hatakeyama, R. Site- and Alignment-Controlled Growth of Graphene Nanoribbons from Nickel Nanobars. *Nat. Nanotechnol.* **2012**, *7*, 651–656.
23. Novoselov, K. S.; Jiang, D.; Schedin, F.; Booth, T. J.; Khotkevich, V. V.; Morozov, S. V.; Geim, A. K. Two-Dimensional Atomic Crystals. *Proc. Natl. Acad. Sci. U. S. A.* **2005**, *102*, 10451–10453.
24. Mak, K. F.; Lee, C.; Hone, J.; Shan, J.; Heinz, T. F. Atomically Thin MoS_2: A New Direct-Gap Semiconductor. *Phys. Rev. Lett.* **2010**, *105*, 136805.
25. Splendiani, A.; Sun, L.; Zhang, Y.; Li, T.; Kim, J.; Chim, C.-Y.; Galli, G.; Wang, F. Emerging Photoluminescence in Monolayer MoS_2. *Nano Lett.* **2010**, *10*, 1271–1275.
26. Radisavljevic, B.; Radenovic, A.; Brivio, J.; Giacometti, V.; Kis, A. Single-Layer MoS_2 Transistors. *Nat. Nanotechnol.* **2011**, *6*, 147–150.
27. Conley, H. J.; Wang, B.; Ziegler, J. I.; Haglund, R. F.; Pantelides, S. T.; Bolotin, K. I. Bandgap Engineering of Strained Monolayer and Bilayer MoS_2. *Nano Lett.* **2013**, *13*, 3626–3630.
28. Lee, H. S.; Min, S. W.; Park, M. K.; Lee, Y. T.; Jeon, P. J.; Kim, J. H.; Ryu, S.; Im, S. MoS_2 Nanosheets for Top-Gate Nonvolatile Memory Transistor Channel. *Small* **2012**, *8*, 3111–3115.
29. Yin, Z.; Li, H.; Li, H.; Jiang, L.; Shi, Y.; Sun, Y.; Lu, G.; Zhang, Q.; Chen, X.; Zhang, H. Single-Layer MoS_2 Phototransistors. *ACS Nano* **2012**, *6*, 74–80.
30. Scott, J. F. *Ferroelectric Memories*; Springer-Verlag: Berlin, 2000.
31. Waser, R. *Nanoelectronics and Information Technology: Advanced Electronic Materials and Novel Devices*; Wiley-VCH: Berlin, 2005.
32. Lee, H. N.; Hesse, D.; Zakharov, N.; Gösele, U. Ferroelectric $Bi_{3.25}La_{0.75}Ti_3O_{12}$ Films of Uniform a-Axis Orientation on Silicon Substrates. *Science* **2002**, *296*, 2006–2009.
33. Van Hai, L.; Takahashi, M.; Sakai, S. Fabrication and Characterization of sub-0.6-μm Ferroelectric-Gate Field-Effect Transistors. *Semicond. Sci. Technol.* **2010**, *25*, 115013.
34. Dubourdieu, C.; Bruley, J.; Arruda, T. M.; Posadas, A.; Jordan-Sweet, J.; Frank, M. M.; Cartier, E.; Frank, D. J.; Kalinin, S. V.; Demkov, A. A.; Narayanan, V. Switching of Ferroelectric Polarization in Epitaxial $BaTiO_3$ Films on Silicon without a Conducting Bottom Electrode. *Nat. Nanotechnol.* **2013**, *8*, 748–754.
35. Batra, I. P.; Wurfel, P.; Silverman, B. D. Depolarization Field and Stability Considerations in Thin Ferroelectric Films. *J. Vac. Sci. Technol.* **1973**, *10*, 687–692.
36. Ishiwara, H. Current Status and Prospects of FET-type Ferroelectric Memories. *J. Semicond. Technol. Sci.* **2001**, *1*, 1–14.
37. Li, H.; Zhang, Q.; Yap, C. C. R.; Tay, B. K.; Edwin, T. H. T.; Olivier, A.; Baillargeat, D. From Bulk to Monolayer MoS_2: Evolution of Raman Scattering. *Adv. Funct. Mater.* **2012**, *22*, 1385–1390.
38. Sinitskii, A.; Dimiev, A.; Kosynkin, D. V.; Tour, J. M. Graphene Nanoribbon Devices Produced by Oxidative Unzipping of Carbon Nanotubes. *ACS Nano* **2010**, *4*, 5405–5413.

39. Ma, T. P.; Han, J.-P. Why is Nonvolatile Ferroelectric Memory Field-Effect Transistor Still Elusive? *IEEE Electron Device Lett.* **2002**, *23*, 386–388.
40. Yusuf, M. H.; Nielsen, B.; Dawber, M.; Du, X. Extrinsic and Intrinsic Charge Trapping at the Graphene/Ferroelectric Interface. *Nano Lett.* **2014**, *14*, 5437–5444.
41. Chuang, S.; Battaglia, C.; Azcatl, A.; McDonnell, S.; Kang, J. S.; Yin, X.; Tosun, M.; Kapadia, R.; Fang, H.; Wallace, R. M.; Javey, A. MoS_2 *p*-type Transistors and Diodes Enabled by High Work Function MoO_x Contacts. *Nano Lett.* **2014**, *14*, 1337–1342.
42. Suh, J.; Park, T.-E.; Lin, D.-Y.; Fu, D.; Park, J.; Jung, H. J.; Chen, Y.; Ko, C.; Jang, C.; Sun, Y.; Sinclair, R.; Chang, J.; Tongay, S.; Wu, J. Doping against the Native Propensity of MoS_2: Degenerate Hole Doping by Cation Substitution. *Nano Lett.* **2014**, *14*, 6976–6982.
43. Dolui, K.; Rungger, I.; Sanvito, S. Origin of the *n*-Type and *p*-Type conductivity of MoS_2 Monolayers on a SiO_2 Substrate. *Phys. Rev. B: Condens. Matter Mater. Phys.* **2013**, *87*, 165402.
44. Sakai, S.; Takahashi, M. Recent Progress of Ferroelectric-Gate Field-Effect Transistors and Applications to Nonvolatile Logic and FeNAND Flash Memory. *Materials* **2010**, *3*, 4950–4964.
45. Lu, H.; Lipatov, A.; Ryu, S.; Kim, D. J.; Lee, H.; Zhuravlev, M. Y.; Eom, C. B.; Tsymbal, E. Y.; Sinitskii, A.; Gruverman, A. Ferroelectric Tunnel Junctions with Graphene Electrodes. *Nat. Commun.* **2014**, *5*, 5518.
46. Fong, D. D.; Kolpak, A. M.; Eastman, J. A.; Streiffer, S. K.; Fuoss, P. H.; Stephenson, G. B.; Thompson, C.; Kim, D. M.; Choi, K. J.; Eom, C. B.; Grinberg, I.; Rappe, A. M. Stabilization of Monodomain Polarization in Ultrathin $PbTiO_3$ Films. *Phys. Rev. Lett.* **2006**, *96*, 127601.
47. Streiffer, S. K.; Eastman, J. A.; Fong, D. D.; Thompson, C.; Munkholm, A.; Ramana Murty, M. V.; Auciello, O.; Bai, G. R.; Stephenson, G. B. Observation of Nanoscale 180° Stripe Domains in Ferroelectric $PbTiO_3$ Thin Films. *Phys. Rev. Lett.* **2002**, *89*, 067601.
48. Geim, A. K.; Grigorieva, I. V. Van der Waals Heterostructures. *Nature* **2013**, *499*, 419–425.
49. Wang, Q. H.; Kalantar-Zadeh, K.; Kis, A.; Coleman, J. N.; Strano, M. S. Electronics and Optoelectronics of Two-Dimensional Transition Metal Dichalcogenides. *Nat. Nanotechnol.* **2012**, *7*, 699–712.
50. Liu, H.; Neal, A. T.; Zhu, Z.; Luo, Z.; Xu, X.; Tománek, D.; Ye, P. D. Phosphorene: An Unexplored 2D Semiconductor with a High Hole Mobility. *ACS Nano* **2014**, *8*, 4033–4041.
51. Lipatov, A.; Wilson, P. M.; Shekhirev, M.; Teeter, J. D.; Netusil, R.; Sinitskii, A. Few-Layered Titanium Trisulfide (TiS_3) Field-Effect Transistors. *Nanoscale* **2015**, *7*, 12291–12296.